SNO-STR-97-039

Testing a Neutron-Activated NaI Detector as a Low-Energy Calibration Device for SNO: Part II

October 27, 1997

M.R. Dragowsky and E.B. Norman
Lawrence Berkeley National Laboratory

Abstract

This report provides further investigation of the utility of ^{24}Na as a calibration source for the Sudbury Neutrino Observatory. A detailed analysis of the escape spectrum of a neutron-activated NaI detector is presented. The response of SNO to the ^{24}Na calibration source is simulated using the SNOMAN Monte Carlo code. It is determined that this technique may provide three low energy calibration points for SNO.

1 Investigation of ^{24}Na in NaI

1.1 Overview

The use of an activated NaI detector as a means to calibrate the Sudbury Neutrino Observatory (SNO) at energies below 5 MeV has been discussed and investigated previously [1]. This method of calibration allows for determination of SNO response at energies which would otherwise be inaccessible due to the large background rate. Knowledge of the response of SNO at these energies will be important when this collaboration addresses the issue of deviation of the shape of the charged current spectrum.

This report offers a detailed analysis of spectra obtained from an activated 7.62 $\times$ 7.62 cm NaI detector in coincidence with a 30 $\times$ 30 cm NaI annulus. The response of SNO to the activated detector has been simulated using SNOMAN. The size of the NaI crystal has been varied to study the response of SNO to differing fluxes of the γs emitted from the decay of ^{24}Na .

1.2 Theory

A NaI detector consists primarily of the isotopes ^{23}Na and ^{127}I . The isotopes ^{24}Na and ^{128}I may be created through thermal neutron activation, and the $t_{1/2}$ are 15 hours and 25.5 minutes, respectively. The decay of ^{24}Na (fig. 1) is by means of β^- decay (Q_-= 5.5 MeV) nearly always followed by the emission of two prompt γ -rays with energies 2.754 and 1.368 MeV (γ_{2754} and γ_{1368}). The maximum energy of the β^- is 1.390 MeV, and it is expected that the β^- will not escape the NaI detector. It is expected that the prompt γ -rays will be detected in one of four ways (Fig. 2):

1. Both γ -rays will deposit full or partial energy in the activated NaI detector.
2. The γ_{2754} will escape and the γ_{1368} will desposit full or partial energy in the detector.
3. The γ_{1368} will escape and the γ_{2754} will desposit full or partial energy in the detector.
4. Both γ -rays will escape.

The signal from the activated detector may be used as a tag to alert the SNO detector to look for Čerenkov photons produced by the emission of either or both of the ^{24}Na γ rays. The possibility of partial energy deposition in the activated detector exists, but with judicious selection of gating in the analysis these events will not effect the performance of the calibration.

1.3 Procedure

A BICRON 7.62 $\times$ 7.62 cm NaI detector was covered by a plastic bag and surrounded by burlap bags filled with polyethylene beads in a shielded enclosure. Two 56 mCi ^{241}Am-Be neutron sources were placed in the enclosure on opposite sides of the bag. Each source provided a neutron flux into 4π of approximately 1.5 $\times$ 10^5 neutrons/second. The sources were 30 cm removed from the detector. The detector was irradiated with neutrons for 24 hours. The activated detector was then placed inside a 30 $\times$ 30 cm NaI annulus and coincidence counting was performed using the activated detector as a tag. The Starburst/CHAOS data acquisition system [2] was used to obtain data over a period of 3 days. A series of three ten minute spectra were taken to demonstrate the decay of ^{128}I during the first half hour of counting, and additional spectra taken over approximately 24 hours were obtained to assess the decay characteristics of the ^{24}Na .

1.4 Analysis

The spectrum obtained from the activated NaI detector is shown in Fig. 3. Four distinct β spectra appear, and are associated with the four conditions identified above. Comparison with the spectra of [1] (Fig. 4) shows that the single peaks in the spectrum at energies of 1.368 and 2.754 MeV are removed. These peaks in the earlier spectrum are due to decays in which the beta energy is not deposited in either detector, and only one gamma deposits energy in the activated detector. We believe this situation occured because there was no attempt to moderate the neutrons emitted from the ^{241}Am-Be neutron source during the earlier investigation. The neutrons are emitted at energies up to 11 MeV, and one must consider the cross-sections of (n,x) reactions on the material of the detector covering and the reflective coating located between the crystal and the cover which may lead to production of ^{24}Na . The detector covering contains aluminum, while the reflective coating is a layer of magnesium oxide packed between the crystal and the cover. Reactions of particular interest are ^{24}Mg (n,p)^{24}Na , and ^{27}Al (n,α)^{24}Na . For neutron energies of 5 MeV these reactions have cross-sections two orders of magnitude greater than that of ^{23}Na (n,γ)^{24}Na . The decay of ^{24}Na in the detector cover or the reflective coating will likely not allow the β to deposit energy in the detector, allowing single energy γ escape peaks to be observed. These are not desirable, as these would be untagged γ in the SNO D_2O .

The spectrum from the NaI annulus clearly shows the γs which escape the activated detector (Fig. 6). Gates were established on the γ peaks of the annulus spectrum to determine which features in the activated spectrum were associated with the emission of the γ_{1368} , γ_{2754} or both γs . Gates were also set on the energy spectrum of the activated dectector and optimised by consideration of three criteria:

1. The ratio of counts in the full energy peak in the annulus to the total triggers in the activated detector gate.

2. The ratio of counts in the full energy peak in the annulus to the total counts in the gated annulus spectrum.

3. The ratio of the full energy peak in the gated annulus spectrum to other full energy peaks.

These criteria lead to the selection of the following gates in the activated detector and provide ratios of γ peaks for use in SNO calibration shown below:

calibration peak	competing peak	ratio calibration/ competing peak	peak/ triggers	peak/ total	energy of gate (MeV)
1368	2754	203:1	.284	.328	2.85-3.27
2754	1368	4.2:1	.265	.276	1.59-2.15
4122	1368	1.2:1	.110	.138	0.69-0.97
4122	2754	1.4:1	.110	.138	0.69-0.97

Table 1: Results of application of selection criteria to data.

These results suggest that a very high signal to noise ratio will be attainable for calibration of SNO with the γ_{1368} (fig. 7). Lower signal to noise ratios are attainable for calibration to the γ_{2754} and the sum peak. The ratios presented rely on the full peak efficiencies of the NaI annulus. It is expected that the full peak efficiency for SNO will be higher. SNO will also provide a true 4π detector geometry. The annulus achieves 93% of 4π for the activated NaI detector, but it also presents short paths for full energy deposition which will not be the case in SNO. Therefore, the ratio of signal to noise presented above should be considered a lower limit. The method of NaI activation by thermal neutrons may be used to produced event rates on the order of 0.1-10 events per second for neutron sources similar to those used in this experiment. The time during which the NaI detector is exposed to the thermal neutron flux will determine the intrinsic event rate, but in this case an exposure time of approximately 24 hours results in 0.9 events per second detected in the sum peak, 1.3 and 2.3 s^{-1} for 2.754 and 1.368 MeV peaks. The efficiency of the NaI annulus to detect full energy peaks in the range of 1-3 MeV is high, but not 100%, therefore these rates should be considered as lower bounds for the geometry and neutron activation scheme used in this experiment. Also, a neutron source of greater intensity may be better suited to irradiation of a calibration source for SNO.

1.5 Additional considerations

1.5.1 Gates

The selection of gate widths in the activated spectrum has been investigated for the purpose of optimizing the ratio of signal to noise for the three ^{24}Na γ peaks. It was assumed that restricting the width of gates would allow for the best signal-to-noise ratio. An investigation of narrow gates on the order of 10 channels in width indicates that there is a lower limit below which the ratio worsens. The reason is as follows: The dominant mode of interaction for a 1-3 MeV γ in a NaI crystal is multiple Compton scattering, therefore, part of the energy of one γ may be deposited in the activated detector, while the remainder of the energy is deposited in the surrounding annulus. The energy may be shared in any ratio. Thus the events which fail to deposit full energy in the annulus are spread over a broad energy region. When one selects a wide gate in the activated detector, one is investigating a large number of Compton events spread across the energy spectrum in the annulus. However, a narrow gate selects a very specific energy range, which in turn selects a small energy range for compton scattered events in the annulus. This leads to the appearance of an additional peak in the annulus due to Compton scattered events at a specific energy. This peak can rival the full energy peaks in intensity when narrow gates are selected (Fig. 8). Since we wish to isolate the full energy peaks as best as possible, overly narrow gates are best avoided. If there were a means to remove the full energy peaks from the annulus spectrum entirely, we could use narrow gates in the activated detector to provide a tunable calibration source through most of the energy range of the γ .

This result suggests that the most straighforward application of the ^{24}Na source in SNO would use a very small NaI crystal. This would minimize the deposition of γ energy in the crystal and maximize the energy deposition in the D_2O . There should then be a strong signal in SNO associated with the sum peak of the two escape γs , and nothing else. This scenario was simulated and the results are provided below in section 2.3. The above results indicate, however, that even when partial energy deposition occurs in the activated NaI detector, very useful signal-to-noise ratios for the single γ lines may be realized, and the results of simulations involving larger crystal sizes are also presented below.

1.5.2 Distribution of Activated Nuclei

The method of calculating diffusion lengths of thermal neutrons in materials specified by Segré [3] has been used to estimate the diffusion length in NaI. A value of 5.7 cm is obtained, using scattering and absorption cross-sections for Na and I from [4] and a value of 3.667 g/cm^3 for the density of NaI crystal [5]. This is on the order of the diameter of the NaI crystal used in this investigation. It is important to use a detector with a crystal of dimension comparable to or less than the thermal neutron diffusion length if the goal is to achieve a uniform distribution of activated nuclei throughout the crystal. Finally, it is worth noting that if one wishes to emphasize the sum peak relative to the individual gamma peaks, to improve the signal for SNO calibration at 4.122 MeV, a crystal with dimensions small compared to the attenuation length of a 1.368 MeV gamma in NaI would be useful. The length to attenuate a beam of 1.368 MeV gammas by 50 percent, as given in [6], is approximately 3.3 cm.

2 Simulation of SNO Response to ^{24}Na Calibration

2.1 Calibration Source

For these simulated experiments the calibration source is composed of a cylindrical NaI detector and a PMT enclosed within a cylindrical shell of stainless steel. The dimensions of the NaI were varied from 3/4"× 3/4" to 4"× 4" to assess the effect of crystal size on the escape spectra of ^{24}Na .

The SNO Monte Carlo and Analysis program (SNOMAN) required only minor modification to allow simulation of the ^{24}Na source. The primary change to SNOMAN was the inclusion of NaI as a valid media. This requires a recompilation of the PEGS4_10.dat file. This process is described in SNO-STR-96-019 and has been accomplished by Steve Biller, who was willing to share his results. It is also necessary to modify the media.dat file to accomodate NaI. The optical properties of NaI were borrowed from acrylic, since SNOMAN will have no cause to propagate Čerenkov photons through NaI.

The ^{24}Na calibration source does not greatly differ in structure from that of the ^{16,17}N calibration source [7]. It consists of a thin cylinder of stainless steel enclosing a source volume optically coupled to a PMT. Therefore, changes to or creation of new geometry files were avoided by making use of the structure of the ^{16,17}N decay chamber. A command file with nomenclature as follows is used to specify the ^{24}Na source geometry:

1. CAN again refers to the outer container of the source.
2. RING denotes the interior space of the container.
3. GAP represents the container of the NaI detector.
4. SCINT is the area filled with NaI.
5. INSTR remains the volume within which the PMT resides.
6. PMT_E remains PMT_E and PMT_I remains PMT_I, and
7. GAS and OPT are not used.

The embedding geometry of SNOMAN for this source is as follows. The interior space (RING) is embedded within the exterior container (CAN). The interior is divided in two, with the upper area (INSTR) containing the PMT, which is divided into an external (PMT_E) and internal region (PMT_I). The lower chamber contains the NaI detector, with no space allowed between the exterior of the NaI and the interior of the exterior wall. Therefore GAP is used to represent the NaI exterior, while SCINT is used for the NaI interior.

The radius and half-height of CAN, RING, GAP and SCINT are varied for each simulation. A wall thickness of 0.1 cm is used for CAN for all simulations. The exterior of the PMT is also taken to have a wall thickness of 0.1 cm. The INSTR and GAP detector elements completely overlap RING, therefore there is no net area for RING in this application. The RING detector element is necessary in this application because of the embedding geometry carried over from the ^{16,17}N source.

2.2 Simulation Scheme

The purpose of the simulation was to study the response of SNO to the ^{24}Na source to determine which of the transitions of ^{24}Na decay may be used as calibration points for SNO. The size of the NaI detector was varied and the nhit spectrum studied to assess the usefulness of each γ line. Each simulation involved 10^5 ^{24}Na decays. The simulations were conducted with the detector at the center of the D_2O volume.

2.3 Results of Simulation

The response of SNO to γ from the decay of ^{24}Na in a 4" $\times$ 4" NaI detector is shown in Figure 9 . The response to γ_{1368} is at much lower nhit than the response to γ_{2754} . This is explained by considering that every γ must lose a minimum amount of energy to lead to production of Čerenkov light. Thus, the γ_{1368} loses a larger fraction of energy than does the γ_{2754} , leading to the greater difference in nhit response. Also, note that the production of Čerenkov photons by e^-s is not a linear process at low e^- energy. The transfer of energy from γ to e^- is effected through either Compton scattering or e^-e^+ production. In the case of Compton scattering, approximately $m_ec^2/2$ is lost. In fact, most Compton scattering will not result in maximum energy transfer. In the case of e^-e^+ production, $2m_ec^2$ is required to form the particle pair. In addition to energy transfer loses, there is also the Čerenkov threshold energy to consider. An e^- must have kinetic energy exceeding .261 MeV to produce Čerenkov photons in D_2O .

Taking these effects together, interactions involving γ_{1368} may only lead to Čerenkov photon production for Compton scattering interactions. At most .902 MeV of e^- kinetic energy will be available for Čerenkov production. The response to the γ_{1368} shows a mean nhit of 4.5. This provides a ratio of 5.0 nhit/Mev. In the case of γ_{2754} , both e^-e^+ production and Compton scattering processes may lead to Čerenkov photon production, but Compton scattering will be dominant. The response to the γ_{2754} shows a mean of 12.7 nhits for an available kinetic energy of 2.25 (1.21) MeV for Compton scattering (e^-e^+ production). This leads to an nhit/MeV ratio of 5.6. Both of these ratios may be compared to the ratio for 6.1 MeV γ from ^{16,17}N , which is 8.9 nhit/MeV. Finally, the case when both γ_{1368} and γ_{2754} deposit energy in SNO results in a mean nhit of 15.7. This case clearly must be considered as simply the sum of the responses of SNO to the individual γs , and not as a calibration point for a single 4.1 MeV γ .

Four sizes of cylindrical NaI crystal were used in the initial simulations, with diameter and height as listed: 4"× 4", 3"× 3", 2"× 2" and 3/4"× 3/4". The nhits spectrum resulting from the simulation of these detectors is provided in Fig. 10 for reference. Three line spectra depicting three energy cuts are shown for each simulation. The cuts are made on the spectrum of energy deposited in the NaI crystal. This information is produced by the EGS4 package within SNO. The cuts are similar to those described in Section 1.4 and are intended to separate the SNO response to the individual γ and the sum peak.

An additional simulation was performed involving a cylindrical NaI detector of dimension 3"× 6". The volume is near to that of the 4"× 4" crystal (695 vs. 824 cm^3). Detectors based on crystals of this size have been available as a standard geometry. The gated spectra resulting from this simulation are shown in Fig. 11. The spectra are comparable in shape and number of events to those of the 3"× 3" and 4"× 4" detectors.

A summary of the simulation results for the sum of γ_{1368} and γ_{2754} is presented in Table 2. Data is presented in both the case of a broad energy gate and an optimal energy gate in the Activated NaI detector. The mean, an estimate of full width at half maximum and the number of events per 10^5 ^{24}Na decays are provided for each calibration point. Similar data from the γ_{2754} and the γ_{1368} calibration are presented in Table 3 and Table 4, respectively.

Crystal	Broad Gate				Optimal Gate			
Size	peak	width	number	energy	peak	width	number	energy
3/4"	15.53	16	84528	0.-1.4	15.60	16	77041	0.-1.0
2"	15.39	16	65713	0.-1.4	15.64	15	54960	0.-1.0
3"	15.30	15	53947	0.-1.4	15.61	15	43695	0.-1.0
4"	15.24	16	44492	0.-1.4	15.57	16	35157	0.-1.0
3"× 6"	14.91	16	47439	0.-1.4	15.3	16	29965	0.-0.8

Table 2: Summary of simulation data for sum of ^{24}Na γs . The mean, FWHM, the number of events per 10^5 ^{24}Na decays and the range of energies (MeV) in the activated NaI energy gate are presented.

Note the low value of the peak for the 3/4" crystal size and γ_{2754} in Table 3. This is because for such a small crystal neither the γ_{1368} nor γ_{2754} is strongly attenuated. The signal

Crystal Size	Broad Gate				Optimal Gate			
	peak	width	number	energy	peak	width	number	energy
3/4”	10.44	13	7896	1.4-2.8	12.21	17	3610	1.4-1.8
2”	10.90	16	17755	1.4-2.8	12.52	15	7512	1.4-1.8
3”	11.21	18	22360	1.4-2.8	12.62	15	8930	1.4-1.8
4”	11.38	18	24783	1.4-2.8	12.52	17	14173	1.4-1.8
3× 6”	11.32	15	23022	1.4-2.8	12.57	15	9162	1.4-1.8

Table 3: Summary of simulation data for ^{24}Na γ_{2754} . The mean, FWHM, the number of events per 10^5 ^{24}Na decays and the range of energies (MeV) in the activated NaI energy gate are presented.

reflects a trigger on Compton scattered γ_{2754} within the crystal. The nhit response is then to the scattered γ and the γ_{1368} which was emitted in coincidence. A hard cut on the NaI energy spectrum is necessary to produce a clean signal, leading to a small number of useful events (7500 events from 10^5 decays).

Crystal Size	Optimal Gate			
	peak	width	number	energy
3/4”	4.84	4	1086	2.8-4.1
2”	4.96	4	3711	2.8-4.1
3”	5.05	4	5668	2.8-4.1
4”	5.01	4	7189	2.8-4.1
3× 6”	4.98	4	6122	2.8-4.1

Table 4: Summary of simulation data for ^{24}Na γ_{1368} . The mean, FWHM and the number of events per 10^5 ^{24}Na decays are presented. The energy range of the gate in the activated NaI detector is 2.8-4.1 MeV.

The shape of the nhits spectrum for the γ_{1368} is insensitive to the width of the energy gate placed on the activated NaI energy spectrum. The energy gate from 2.8-4.1 MeV produces the same shape as that for any narrower gate within this range. This is true independent of the size of the crystal. The number of γ_{1368} events is then directly determined by the crystal size. A small crystal minimizes the number of γ_{1368} events, while a large crystal maximizes these events.

The preceeding discussion is helpful in considering the utility of ^{24}Na as a source of multiple calibration points for SNO. In the assessment of ^{24}Na described in Section 1.4 ratios of peaks to background were assessed (Fig. 7). It was asserted that the ratios obtained were lower limits. Similar spectra are presented in Fig. 12. As seen in these results of the Monte Carlo, SNO clearly distinguishes between the three peaks. With appropriate selection of energy gates in the activated NaI spectrum, the SNO response to these three γ escape energy peaks may be separately obtained.

3 Conclusion

The feasability of calibrating SNO for energies below 5 MeV through use of a neutron activated NaI detector has been investigated and quantified. Such a source can be prepared above ground and can be sealed to avoid contamination to the SNO D_2O . Expected counting rates have been provided, but these may be adjusted through the level of activation achieved in, as well as the size of, the NaI detector. Activation of the detector with thermal neutrons should be performed to provide a spectrum free of untagged gamma rays. Discussions are currently underway to make use of high intensity beams of thermal neutrons at Chalk River. A count rate of 1,000 Hz may be easily obtained with this source.

SNO responds well to the case when both ^{24}Na γ emerge from the calibration source, regardless of the size of the detector. A peak appears at 15 nhits. This peak is enhanced by using the smaller NaI size, but remains a main feature in the nhit spectrum for each crystal size in the study. The larger crystal provides more attenuation of the γs and leads to an enhancement of the signal for the individual γs .

What was not apparent from the previous work [1] is how close together the nhit peaks for the sum and γ_{2754} spectra would be. Recognizing that SNO is not sensitive to the sum of the γ energy, but rather the sum of the Čerenkov light produced separately by γ_{1368} and γ_{2754} , leads to the conclustion that the NaI detector ought to be made large enough to attenuate the γs such that reasonable detection rates for the single γs may be obtained. The sum peak may still be assessed in the context of a higher energy γ which undergoes multiple scattering and leads to deposition of approximately 3 MeV of e^- kinetic energy in SNO, but the single γ spectra from the individual γs will be of significant value for specifying the response of SNO to low energy neutrino events.

References

[1] Testing a Neutron-Activated NaI Detector as a Low-Energy Calibration Device for SNO. E.B. Norman, I. Zlimen, and R.M. Larimer, LBNL, SNO-STR-93-032, Sept. 13, 1993.

[2] Starburst/CHAOS Operators Manual

[3] E. Segre, Nuclei and Particles, W.A. Benjamin, Inc, pp 534-49, 1965.

[4] Neutron News, Vol. 3, No. 3, pp 29-37, 1992 and http://ne43.ne.uiuc.edu/n-scatter/n-lengths/.

[5] CRC Handbook of Chemistry and Physics, 52nd Edition, p. B-158.

[6] NaI(Tl) Scintillation Detectors, J.G. Bellian and R.R. Dayton, Bicron Corporation, 1974.

[7] Simulation of the ^{16,17}N Decay Chamber, M.R. Dragowsky, Y.D. Chan, E.B. Norman and C.E. Okada, SNO-STR-97-xxx, Aug. 19, 1997.

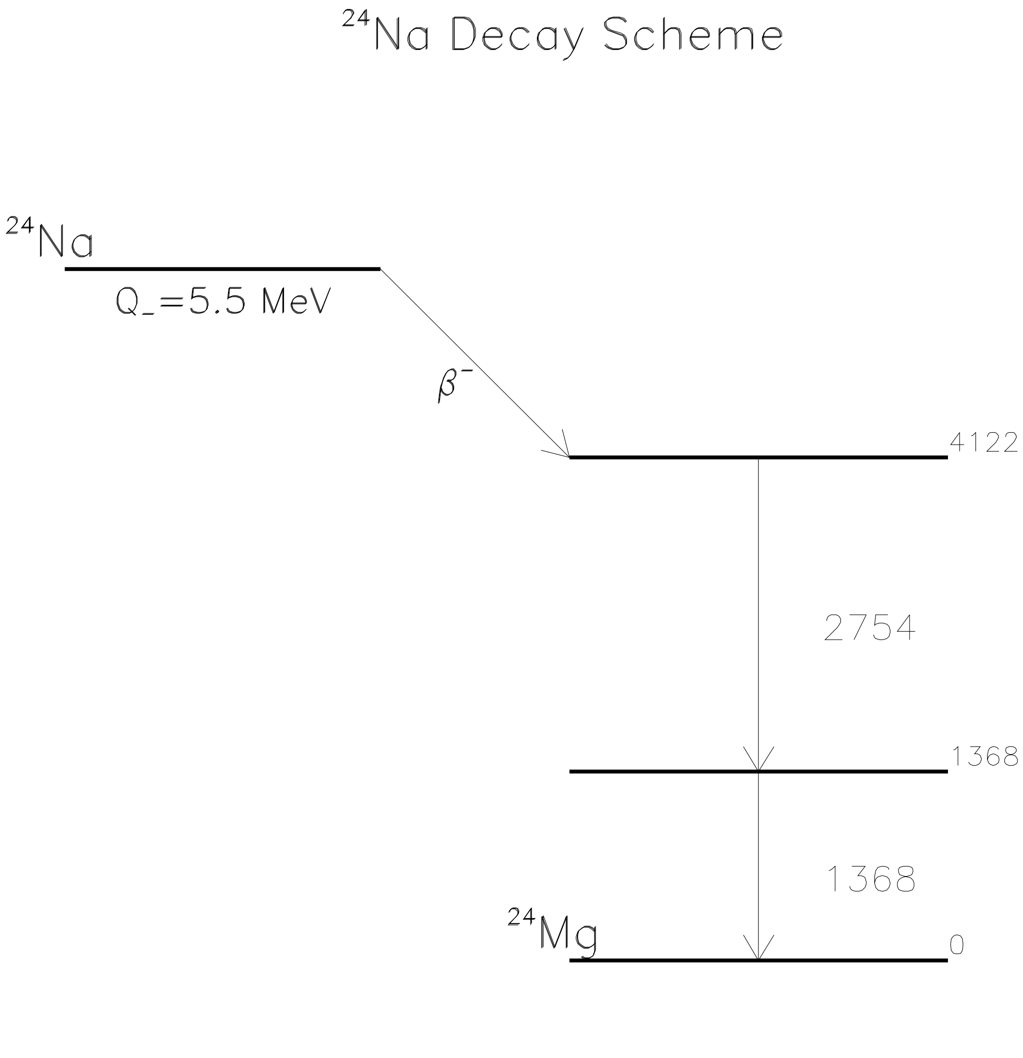

Figure 1: The decay scheme of ^{24}Na .

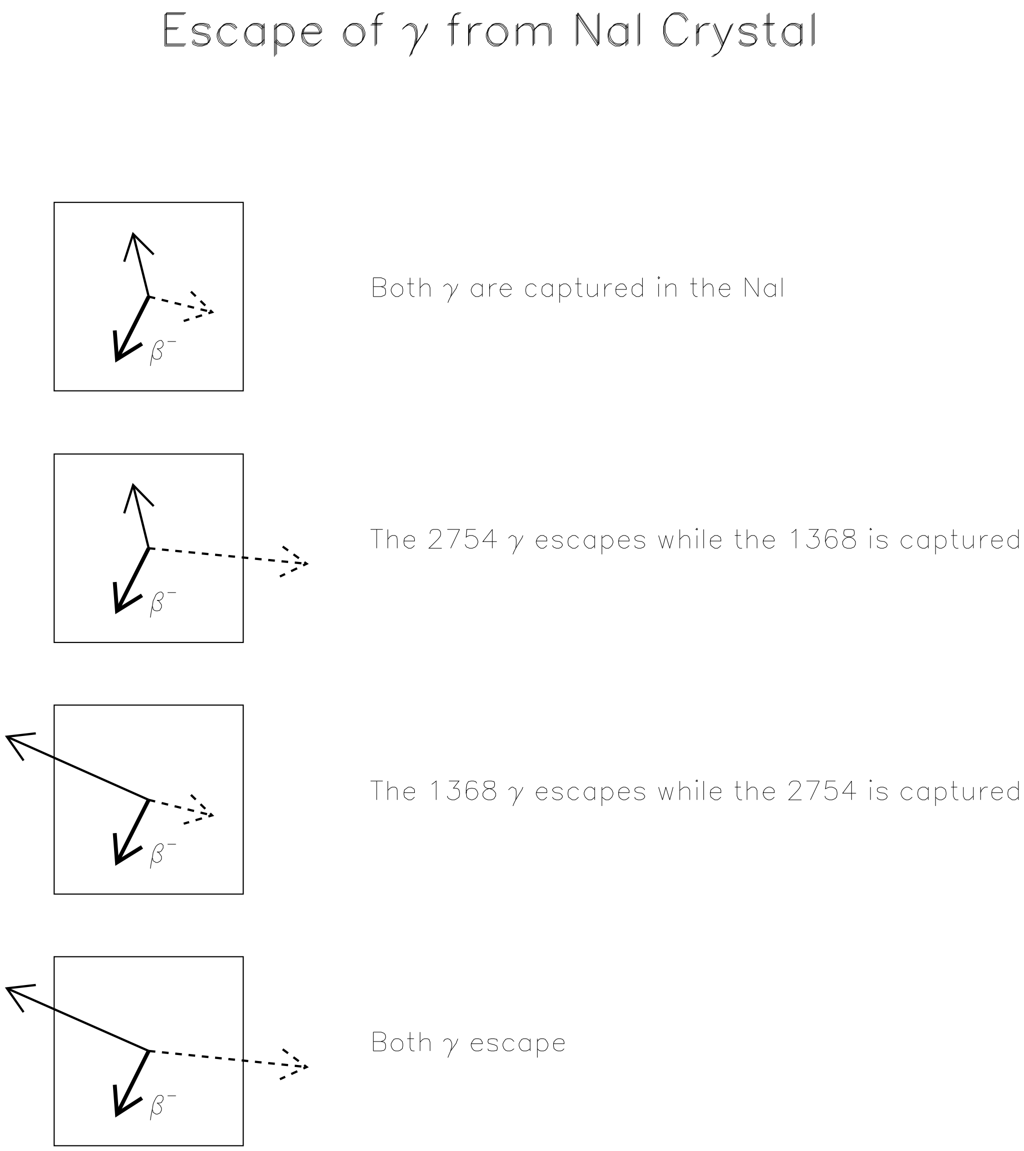

Figure 2: Schematic of coincidence detection of ^{24}Na .

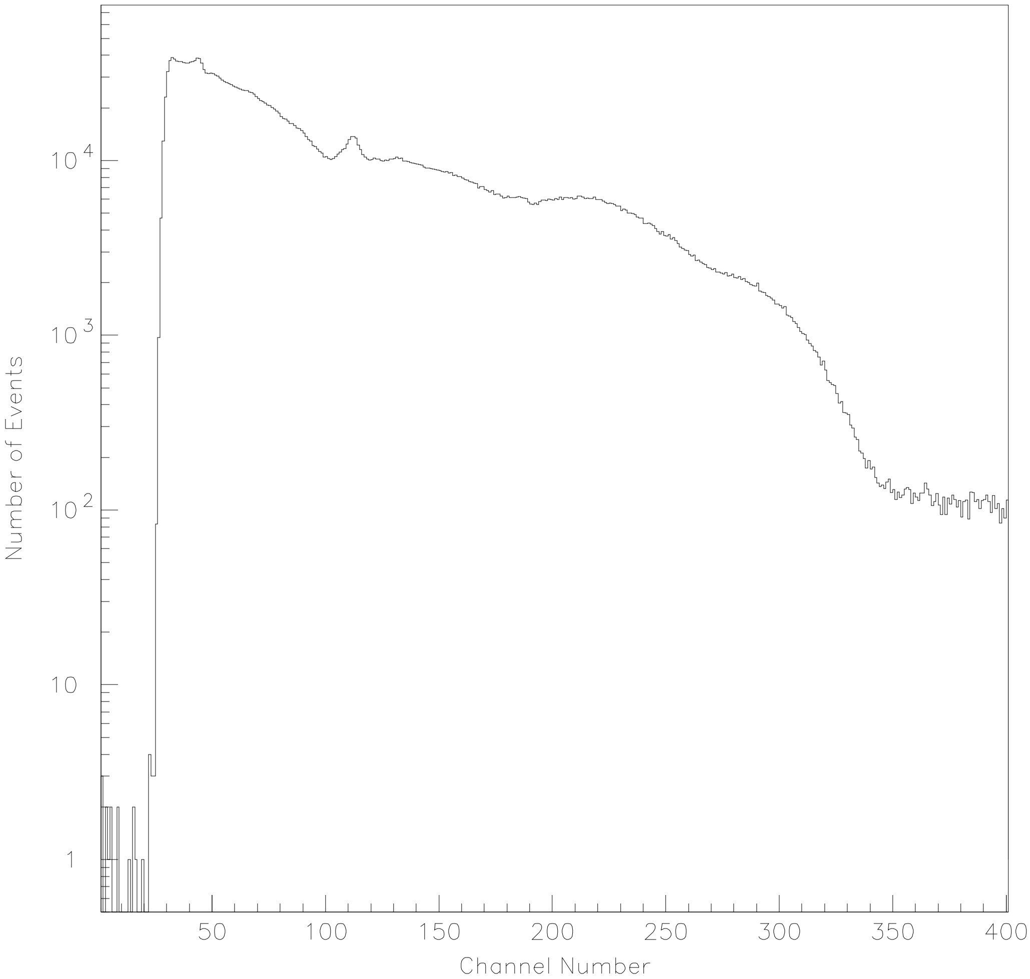

Figure 3: Spectrum of thermal neutron activated NaI detector. The peak at channel 112 is due to ^{40}K.

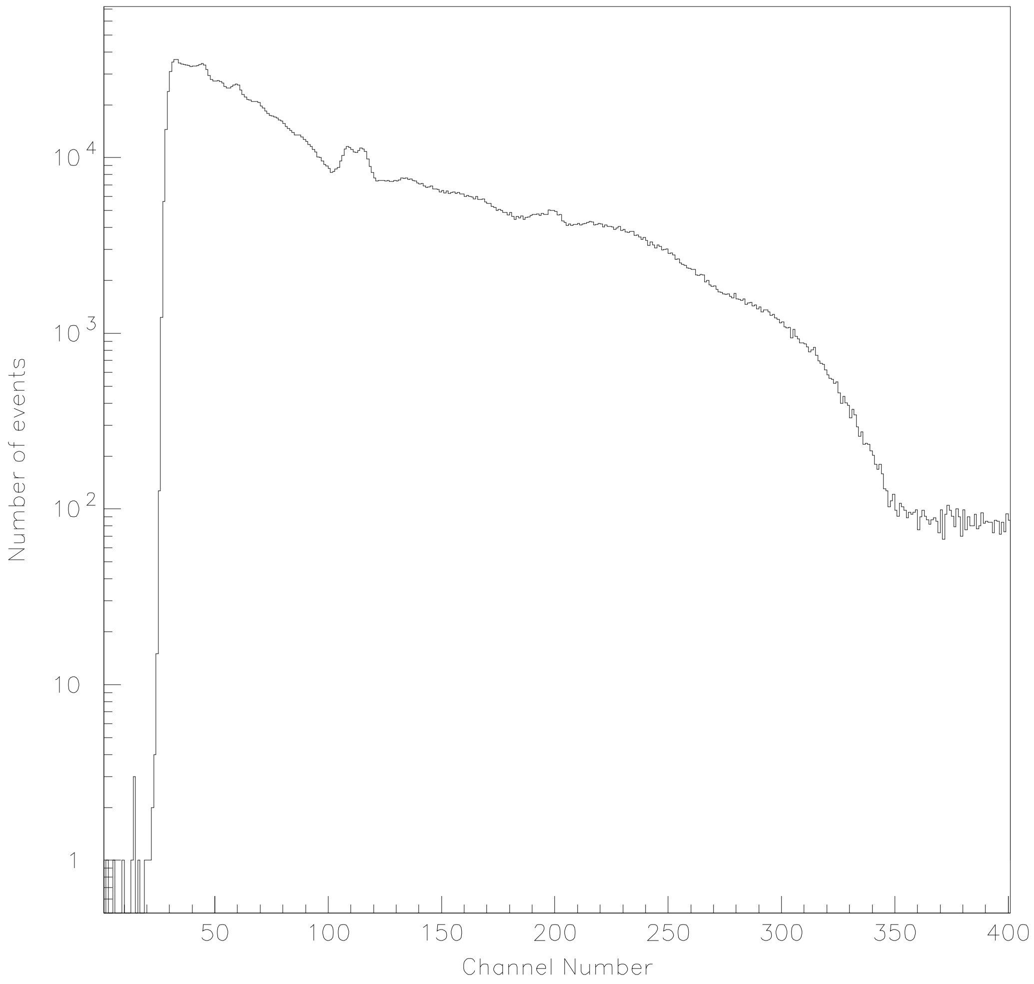

Figure 4: Spectrum of NaI detector exposed to broad spectrum neutron source.

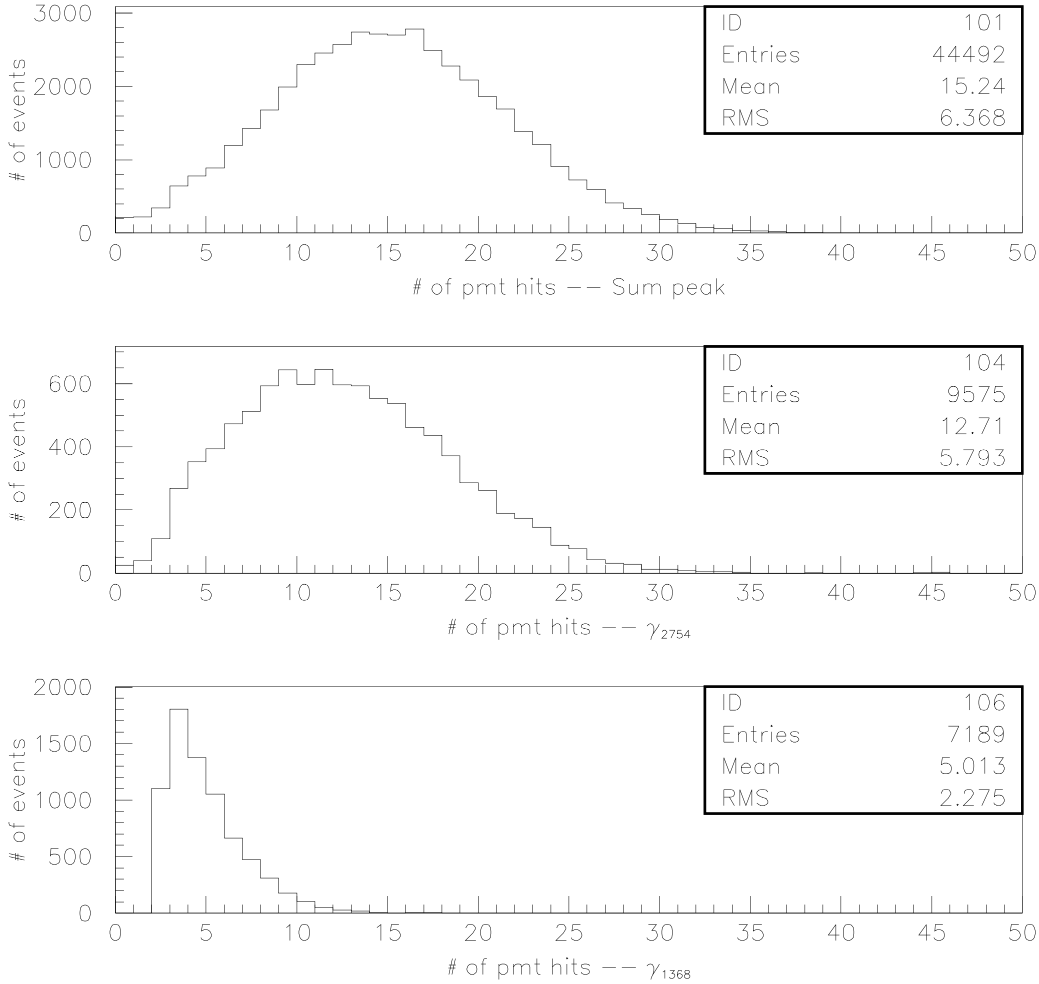

Figure 5: Individual spectra resulting from SNOMAN simulation of 4”× 4” NaI crystal.

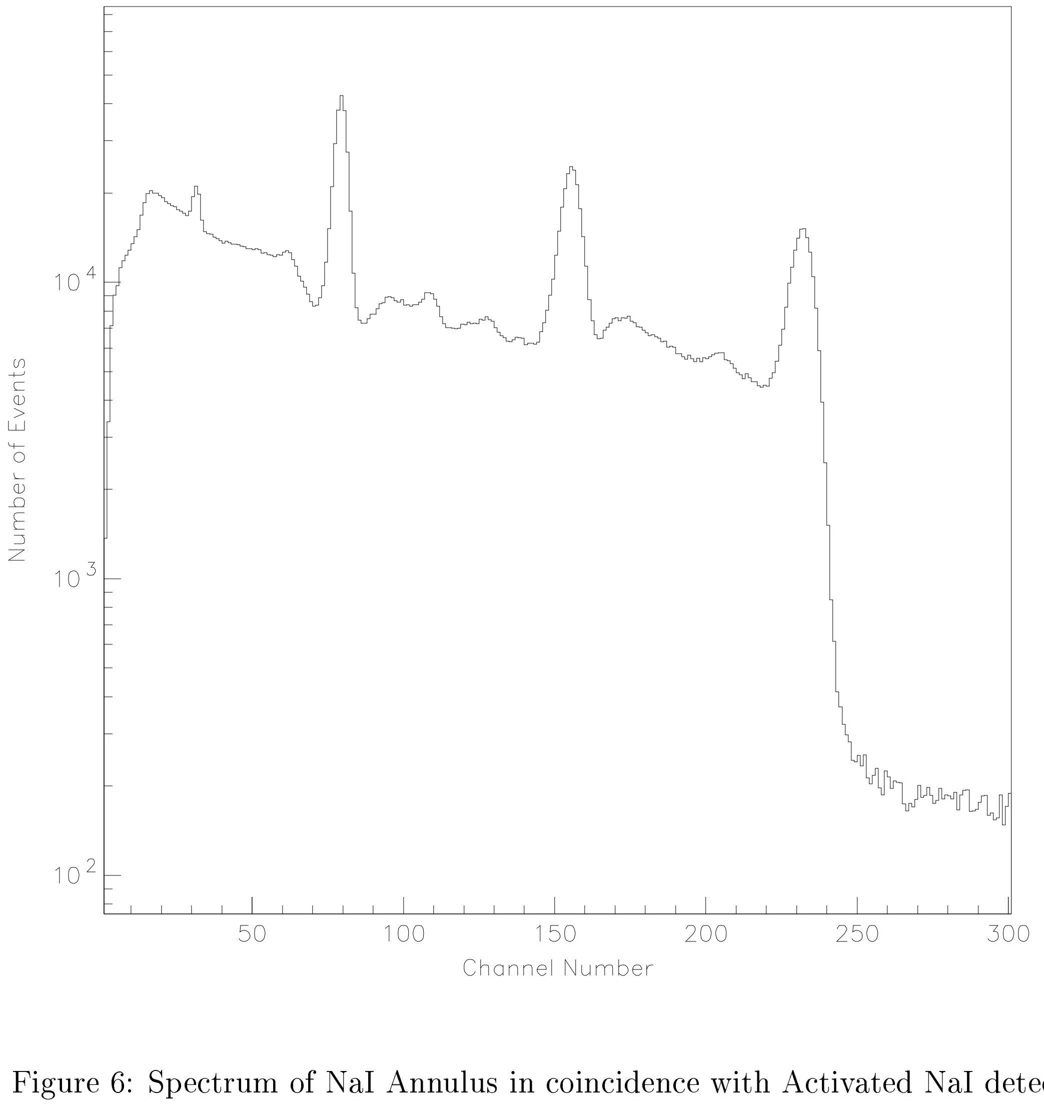

Figure 6: Spectrum of NaI Annulus in coincidence with Activated NaI detector.

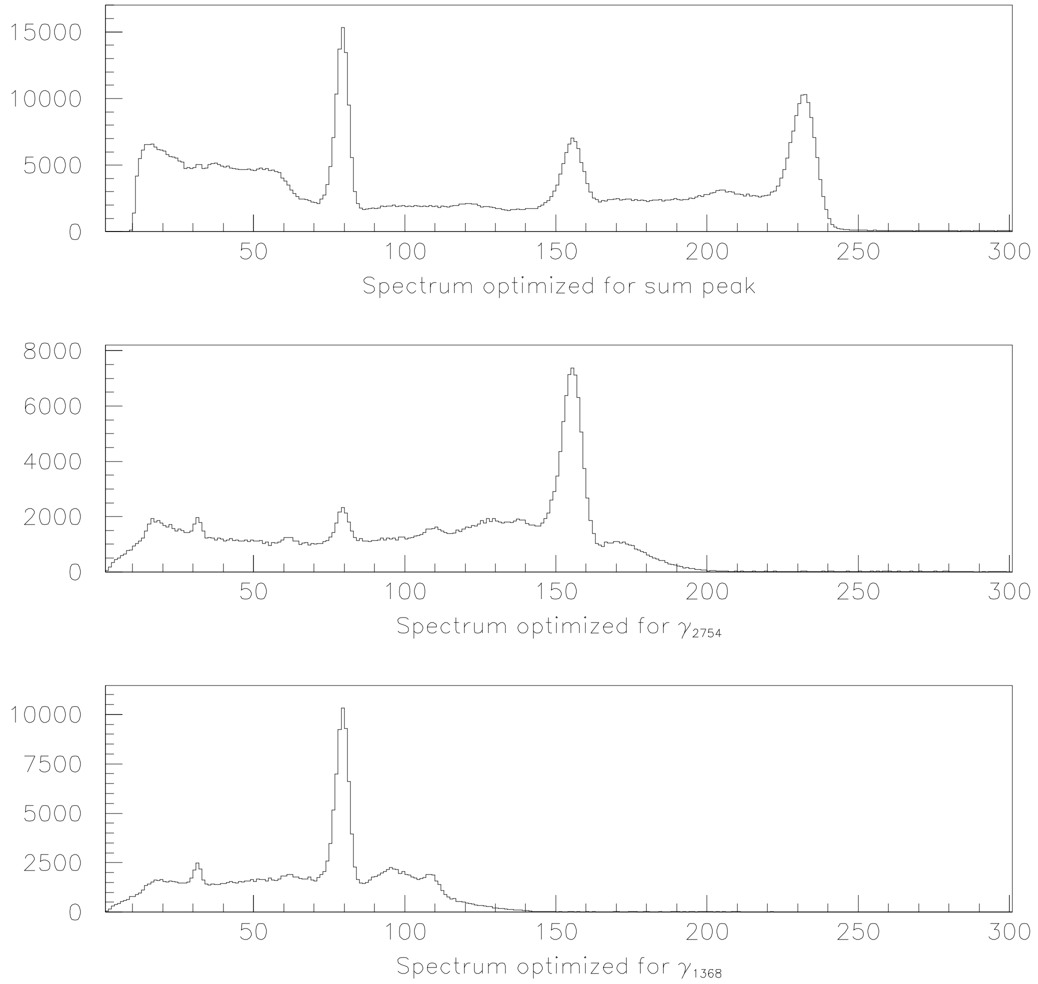

Figure 7: Escape peak spectra resulting from optimized gating. Channel number is displayed on the abscissa.

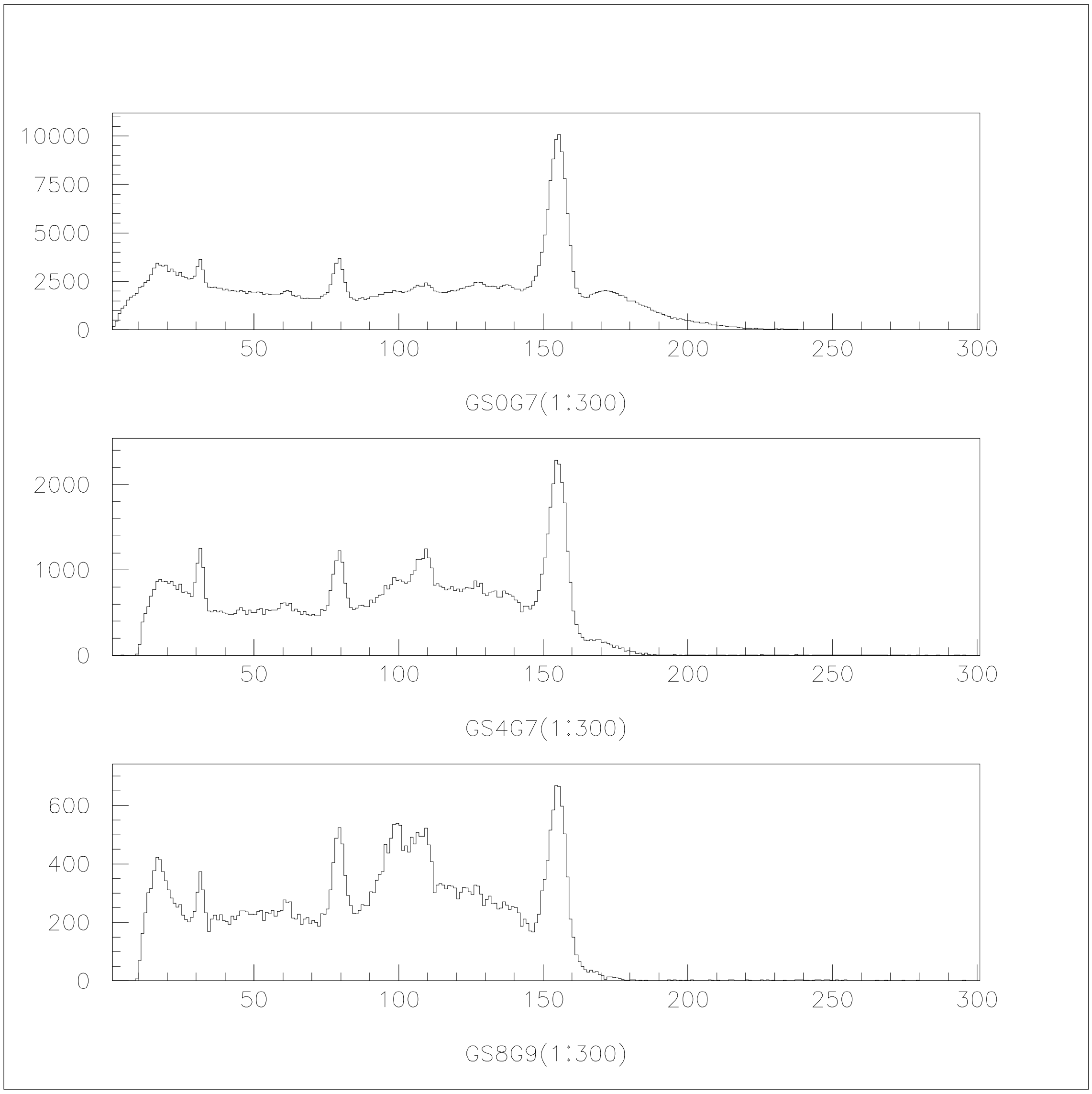

Figure 8: Comparison of spectra of NaI Annulus for gates of decreasing width. The designations GS*G# denote vector identifiers for the displayed spectra within PAW. Channel number is displayed on the abscissa.

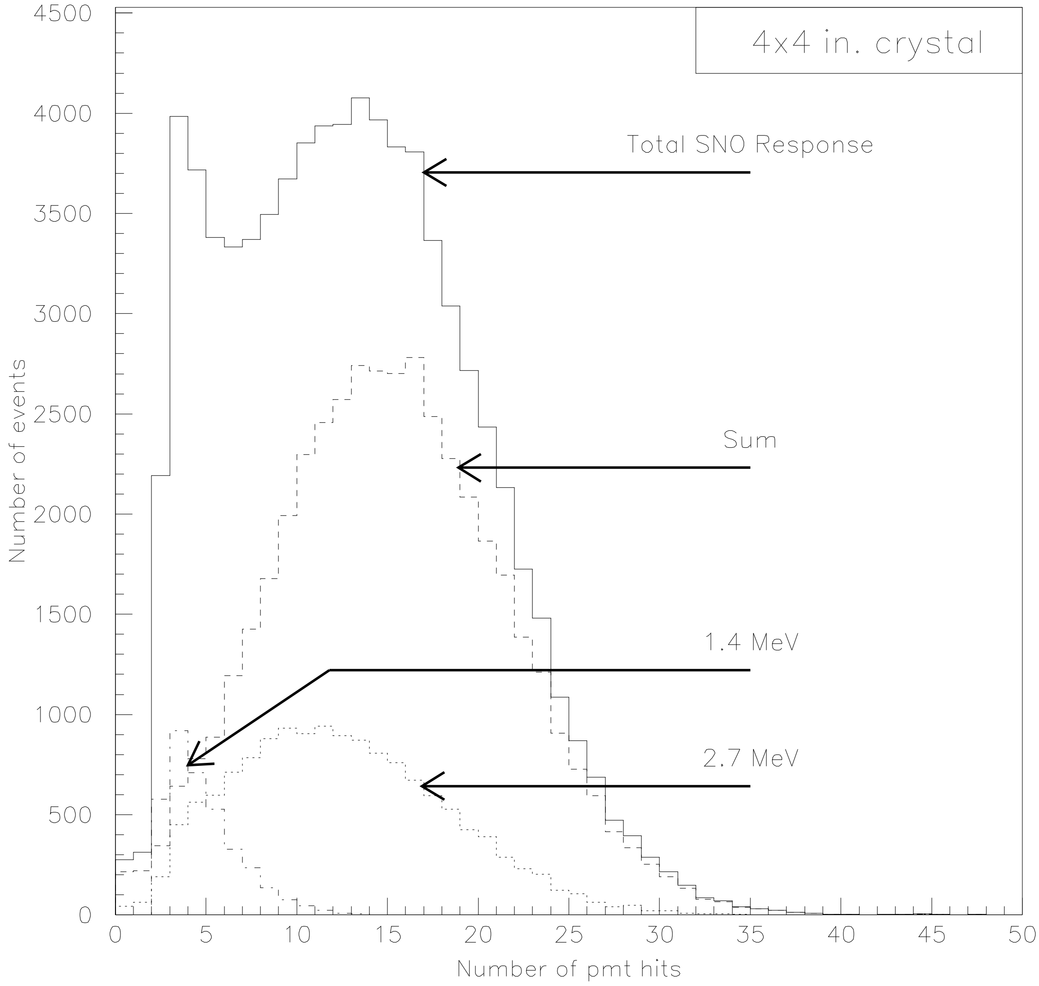

Figure 9: Spectra resulting from SNOMAN simulation of 4"× 4" NaI crystal. Energy cuts have been used to produce the three spectra which appear with dashed lines.

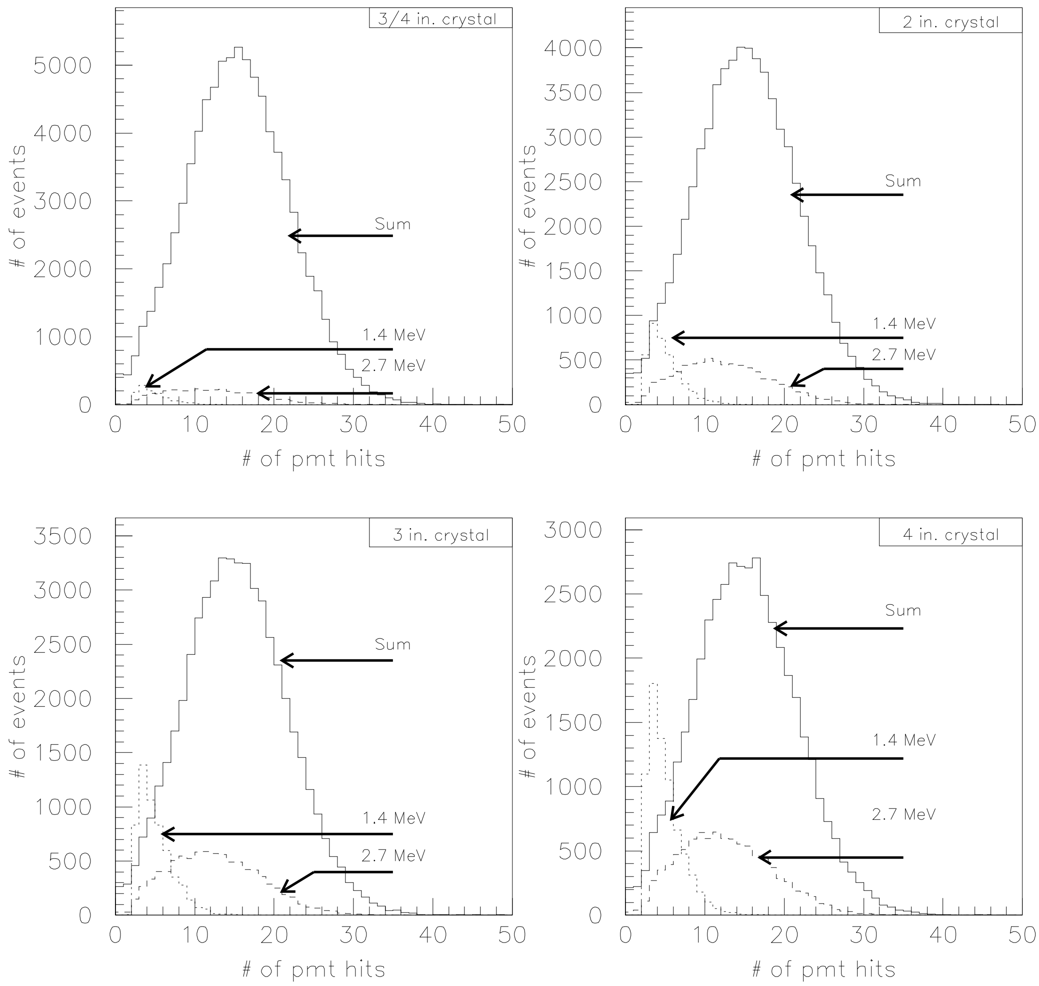

Figure 10: Simulated SNO response to four sizes of NaI crystal. The spectra appearing in each plot are the result of energy cuts on the activated NaI spectrum. As crystal size increases, the SNO response to the individual γs grows.

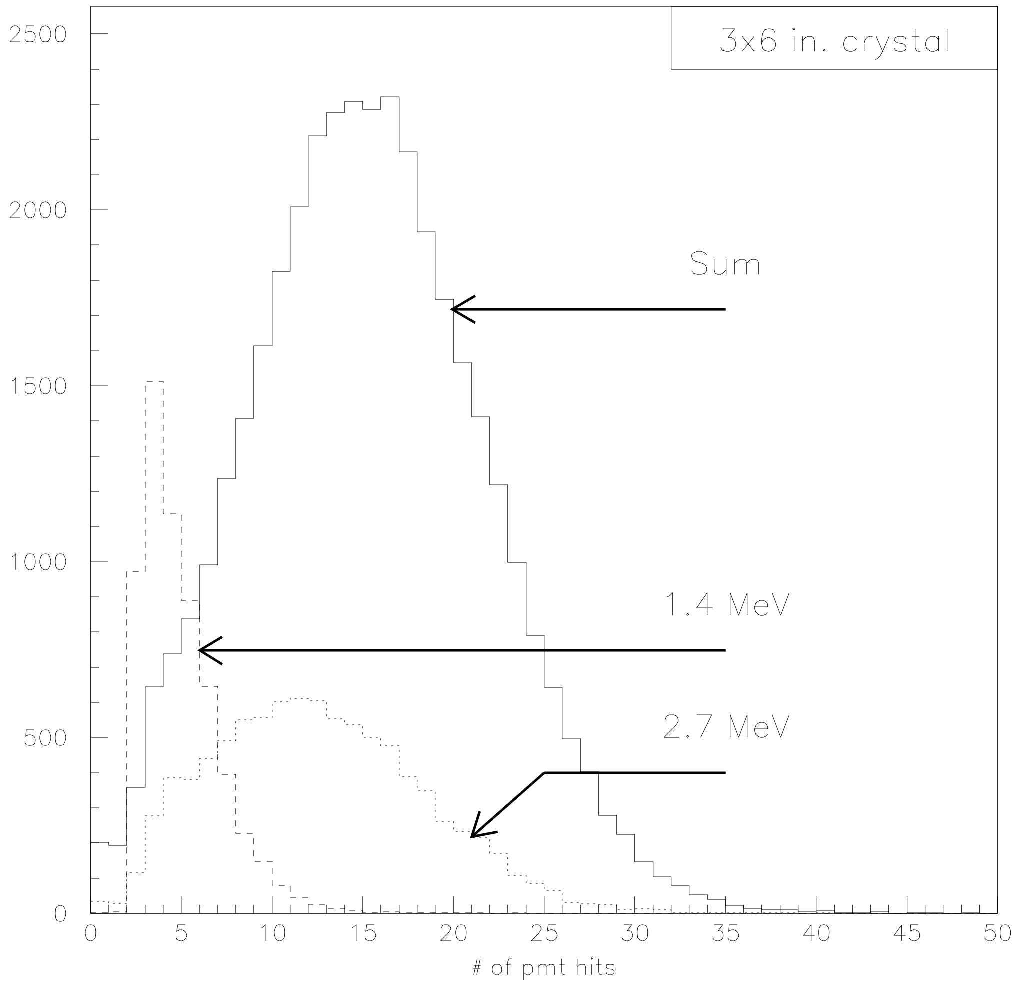

Figure 11: Simulated SNO response to 3"× 6" cylindrical NaI crystal.

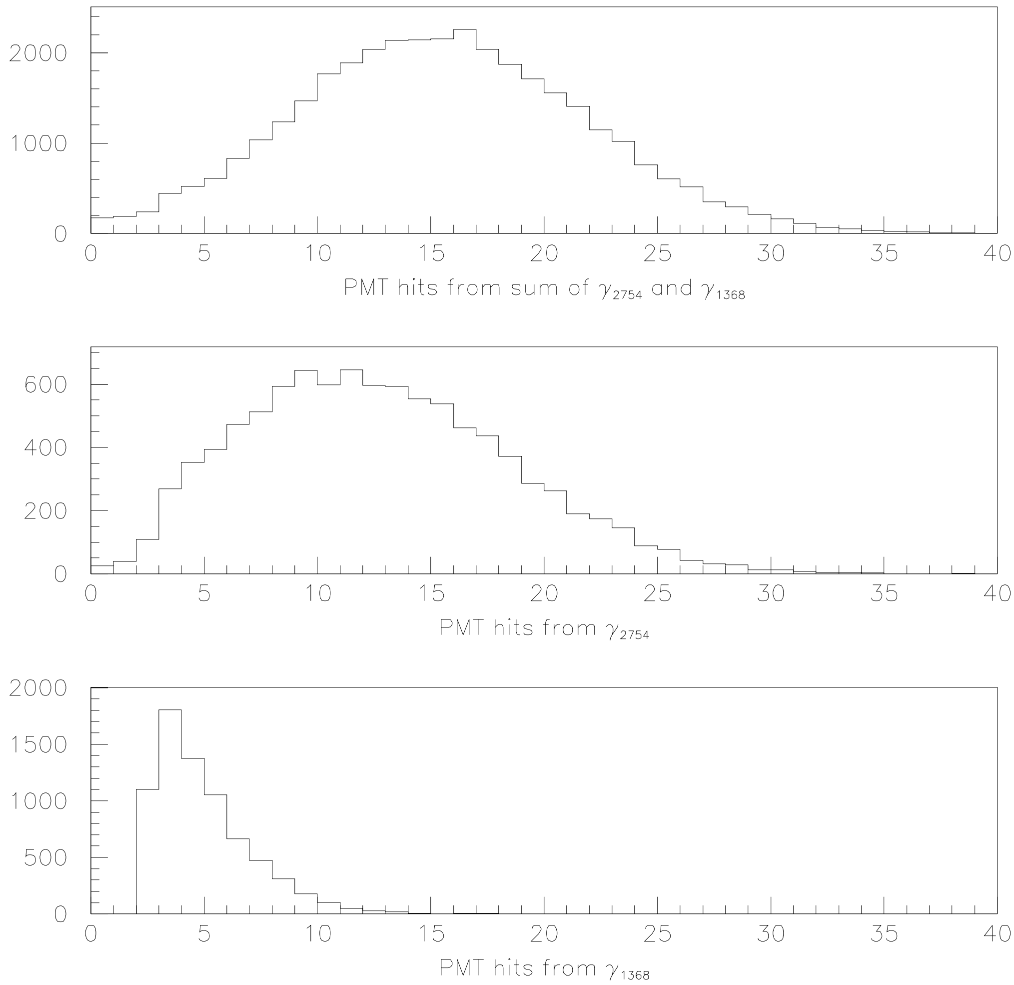

Figure 12: Simulated SNO response to energy cuts placed on the spectrum of energy deposited in a 4"× 4" activated NaI crystal.